Hydrol. Earth Syst. Sci. Discuss., 10, 855–893, 2013
www.hydrol-earth-syst-sci-discuss.net/10/855/2013/
doi:10.5194/hessd-10-855-2013

Hydrology and Earth System Sciences Discussions

Assessing hydrological model behaviors by intercomparison of the simulated stream flow compositions: case study in a steep forest watershed in Taiwan

J.-C. Huang[1], T.-Y. Lee[1], J.-Y. Lee[1], S.-C. Hsu[2], S.-J. Kao[2,3], and F.-J. Chang[4]

[1]Department of Geography, National Taiwan University, Taipei, Taiwan
[2]Research Center for Environmental Changes, Academia Sinica, Taipei, Taiwan
[3]State Key Laboratory of Marine Environmental Science, Xiamen University, Xiamen, China
[4]Department of Engineering for Sustainable Environment, National Taiwan University, Taiwan

Received: 5 December 2012 – Accepted: 2 January 2013 – Published: 18 January 2013

Correspondence to: J.-C. Huang (riverhuang@ntu.edu.tw)

Published by Copernicus Publications on behalf of the European Geosciences Union.

Abstract

The accurate stream flow composition simulated by different models is rarely discussed, and few studies addressed the model behaviors affected by the model structures. This study compared the simulated stream flow composition derived from two models, namely HBV and TOPMODEL. A total of 23 storms with a wide rainfall spectrum were utilized and independent geochemical data (to derive the stream composition using end-member mixing analysis, EMMA) were introduced. Results showed that both hydrological models generally perform stream discharge satisfactory in terms of the Nash efficiency coefficient, correlation coefficient, and discharge volume. However, the three simulated flows (surface flow, interflow, and base flow) derived from the two models were different with the change of storm intensity and duration. Both simulated surface flows showed the same patterns. The HBV simulated base flow dramatically increased with the increase of storm duration. However, the TOP-derived base flow remained stable. Meanwhile, the two models showed contrasting behaviors in the interflow. HBV prefers to generate less interflow but percolates more to the base flow to match the stream flow, which implies that this model might be suited for thin soil layer. The use of the models should consider more environmental background data into account. Compared with the EMMA-derived flows, both models showed a significant 2 to 4 h time lag, indicating that the base-flow responses were faster than the models represented. Our study suggested that model intercomparison under a wide spectrum of rainstorms and with independent validation data (geochemical data) is a good means of studying the model behaviors. Rethinking the characterization of the model structure and the watershed characteristics is necessary in selecting the more appropriate hydrological model.

HESSD

10, 855–893, 2013

1 Introduction

Simulating the stream flow accurately is one of the main concerns of scientists and managers, particularly in hydrology science and water resource assessment. For this goal, hydrological models are implemented through different conceptualizations of simplified representations of the real world (Beven, 2001; Refsgaard and Henriksen, 2004). Therefore, a number of hydrological models with different model structures have been proposed and applied around the world. Undoubtedly, this significant progress in hydrological modeling works has enabled the discharge simulation capability facilitating many applications. Currently, the attentions shift to understanding more on the model structure and the corresponding behaviors for advanced interpretations (Reed et al., 2004; Clark et al., 2008). For example, some previous studies applied different model structures (e.g. runoff generations or routings) on the same catchment to determine the suitability and applicability of a model (Winchell et al., 1998; Valeo et al., 2001; Johnson et al., 2003). These comparative studies revealed that models with different structures could satisfactorily simulate the stream discharge for the same catchment. However, the selection of the hydrological models and the model structure uncertainties are still not fully understood. Recently, Clark et al. (2008) have applied 79 unique model structures by combining the components of four existing hydrological models into catchments. They concluded that the model structure uncertainty is as important as the parameter uncertainty, indicating that intercomparison among models can give insight into the understanding of hydrological models. In addition, Weiler et al. (2003) integrated the instantaneous unit hydrograph and the temporal variability of rainfall isotopic composition to interpret the runoff processes and pathways. The series of studies conducted by the McDonnell's laboratory demonstrated that the transit time plays a crucial role in testing the hydrological models and indicated the importance of geochemistry on hydrological modeling (Fenicia et al., 2008; Sayama and McDonnell, 2009).

HESSD
10, 855–893, 2013

Although the abovementioned studies made a significant step forward on the hydrological model choice and suitability, the accuracy of the simulated stream flow composition controlled by different model structures still needed further studies. Such result raises two interesting issues. (1) Why does the model prefer to provide such discharge composition? (2) What kind of discharge composition from the models is relatively realistic or reliable? Obviously, the model preference or model behavior is dominated by the model structure, governing equations, and calibration. Therefore, this study incorporated the same base-flow equation (linear reservoir concept) into the different model structures (HydrologiskaByråns Vattenbalansavdelning – HBV – and TOPMODEL) to investigate the influence of the model structure on the simulations. Because the discharge composition indicates the different runoff flow paths and relevant hydrogeomorphic processes (Wagener et al., 2010), understanding the two questions not only provides insight into hydrology but also on water resource planning.

To investigate the two model behaviors, hourly rainstorm events covering a wide rainfall spectrum were used. This study applied the two hydrological models with the same base-flow component to a steep mountainous watershed in Taiwan. Altogether, 23 events since 1986 to 2011 were used to calibrate the well-performed parameter sets. Based on the two modeling results and retrieved parameters, the model applicability was evaluated in terms of efficiency coefficient, volume bias ratio, and correlation coefficient. Meanwhile, the stream flow compositions derived from the two models were intercompared to investigate the model behaviors during the different events. Finally, the two rainstorms, supplemented by an intensive geochemical dataset, were independently introduced to assess and validate the simulated stream flow composition. This study improved our understanding on the model choice and the role of the parameters in the different runoff simulation, as well as shed light on the modeling improvement.

HESSD
10, 855–893, 2013

2 Materials and methods

2.1 Study area

This study chose the Chi-Chia-Wen watershed in central Taiwan, a typical forested, steep, and mountainous watershed with a drainage area of 105 km^2 (Fig. 1). The elevation varies from 1131 m to 3882 m a.s.l. (above sea level), and the steep slope (average of approximately 33.3°) represents a high runoff velocity and sediment transport (Kao et al., 2011; Lee et al., 2012). In this watershed, the original and secondary forests occupy approximately 87 % of the area. Some agricultural lands (e.g. orchard and vegetable farms) spread along the riparian zone. The average annual precipitation here is 2107.3 mm (based on 1956–2002 data) and varies with distinct seasonality. Approximately 75 % of the annual precipitation occurs during the wet season (May to October), and tropical cyclone (typhoon) is the main contributor. The annual discharge is approximately 1816.9 mm (from 1974–2001 data), with a mean daily discharge of 7.94 $m^3 s^{-1}$. The annual average air temperature is 15.8 °C, and the monthly average air temperatures in January and July are 4 and 23 °C in 2000–2009 (Huang et al., 2006).

For the rainstorms, a total of 23 rainstorms with significant stage rise (over 2 m) were selected to evaluate the applicability of the two hydrological models (Table 1). In general, the total rainfall ranged from 184.5 to 836.4 mm, with a maximum rainfall intensity of from 10.7 to 39.5 mm h^{-1}. The average cumulative rainfall was approximately 430 mm within 102 h. The total runoff depth ranged from 37.8 mm to 672.6 mm and was significantly positively correlated with the total rainfall and rainfall duration. The peak discharges ranged from 2.28 to 17.5 mm h^{-1} and were positively correlated with the total rainfall, average rainfall intensity, and maximum rainfall intensity (Table 1). The stream discharge responded rapidly to the rainfall within a short time lag (generally less than 2 h) showing a short travel time. These events, which crossed a wide spectrum in terms of the total rainfall, are the critical factors that detect the limit of model applicability.

HESSD
10, 855–893, 2013

2.2 Hydrological modeling: TOPMODEL and HBV

The two hydrological models (HBV, HydrologiskaByråns Vattenbalansavdelning, and TOPMODEL, hereafter TOP) were used in this study. Both models are regarded as conceptual distributed models and have been widely applied in many studies. Here, we briefly introduced the two models.

2.2.1 HBV model

The HBV model was originally developed by the water balance section of the Swedish Meteorological and Hydrological Institute and has been modified into several versions (e.g. Bergström and Forsman, 1973; Bergström, 1992; Lindström et al., 1997; Krysanova et al., 1999; Haberlandt et al., 2001; Blöschl et al., 2008). Recently, Aghakouchak and Habib (2010) modified this model into a distributed-based model, and we used this version in the current study. The HBV model consists of four modules: (1) snowmelt and snow accumulation, (2) soil moisture and effective precipitation, (3) evapotranspiration, and (4) runoff response. For rainstorm (short-term) simulation, the hourly time step was used. In this study, the snow accumulation, snowmelt, and evapotranspiration modules were turned off. Because this study site, in the high elevation (> 3000 m), almost none or very little snow appears during subtropical summer. Meanwhile, the amount of evapotranspiration during rainstorms is relatively small compared with the total precipitation. Therefore, the two modules can be neglected. The considered processes of the HBV model are shown in Fig. 2a. In the HBV model, precipitation is usually divided into two components: the first contributes to the soil root zone, and the second contributes to the interflow storage. The second component is usually known as effective precipitation. This component is estimated by an exponential coefficient and the saturation in the soil root zone. In the soil root zone, saturation is defined as the soil moisture over the field capacity (FC), the parameter that describes the maximum water storage. Adopting this concept, the higher the saturation is, the larger is the precipitation proportion recharged into the inter flow storage. Equation (1)

HESSD
10, 855–893, 2013

describes the calculation of the effective precipitation, which is a function of the current soil moisture content.

$$P_{\text{eff}} = P \cdot \left(\frac{\text{SM}}{\text{FC}}\right)^{\beta} \tag{1}$$

where P_{eff} is the effective precipitation [L], SM is the actual soil moisture [L], FC is the maximum soil storage capacity [L], P is the hourly precipitation [L], and β is a model parameter (shape coefficient) [–]. The soil moisture that received rainfall dynamically changes over the simulation time steps. An initial value of the soil moisture is required to start the calculations.

The interflow and base-flow estimations at the watershed outlet are based on the linear reservoir concept. Two conceptual reservoirs are involved: one is for the interflow, and the other is for the base flow (Fig. 2a). The reservoirs are directly connected to each other by a constant percolation rate (P_{r}). Figure 2a shows two outlets (Q_{s} and Q_{i}) in the upper reservoir and one outlet (Q_{b}) in the lower reservoir. When the water level in the upper reservoir exceeds the threshold value (L) in the upper reservoir, surface runoff (Q_{s}) occurs quickly from the upper reservoir. For the surface flow routing, the unit response function implemented by the diffusive transport approach is used (Liu et al., 2003; Huang et al., 2009). Meanwhile, the water level in the upper reservoir responds to generate the interflow (Q_{i}). The base-flow response in the lower reservoir is relatively slower and controlled by the water level in that reservoir. The recession coefficients K_{s}, K_{i}, and K_{b}, control the response functions of the three flows. The three recession coefficients and the percolation rates are all model parameters, which are estimated via calibration. The three flows in the outlet are illustrated in Eqs. (2) and (3) as follows:

$$Q_{\text{s}} = \begin{cases} K_{\text{s}}(S_{\text{i}} - L)A_{\text{c}} & \text{if } S_{\text{i}} > L \\ 0 & \text{if } S_{\text{i}} < L \end{cases} \tag{2}$$

$$Q_{\text{b}} = A \cdot K_{\text{b}} \cdot S_{\text{b}} \quad Q_{\text{i}} = A \cdot K_{\text{i}} \cdot S_{\text{i}} \tag{3}$$

HESSD
10, 855–893, 2013

where Q_s, Q_i, and Q_b represent the surface flow, interflow, and base flow [L^3T^{-1}], respectively. The parameters K_s, K_i, and K_b are the storage coefficients of the surface flow, interflow, and base flow [T^{-1}], respectively. S_i is the upper reservoir water level [L], S_b is the lower reservoir water level [L], and L is the threshold water level [L]. A and A_c are the watershed and cell areas [L2], respectively. The total simulated runoff is obtained by adding the three flows.

2.2.2 TOPMODEL

TOPMODEL proposed by Beven and Kirkby (1979) and has been applied widely around the world (Beven, 1996). The kernel feature of this model is to use the topographic index (defined as the contributing area over the gradient) to estimate the variable source area and then simulates the discharges. Because of its concise structure, numerous modifications have been introduced in the past three decades. We used the three-layer TOP (Huang et al., 2009) in this study. This modification has been widely used in Taiwan for relevant hydrological applications either for hourly or for daily time step input (Huang et al., 2011, 2012). The conceptual scheme is shown in Fig. 2b. This model divides the soil column into three layers: upper, middle, and bottom layers, to simulate the surface flow, interflow and base flow, respectively (composing the stream discharge). In this model, the following 9 parameters need calibration: maximum root zone storage (S_{rmax}), initial root zone storage (S_{r0}), Mannings' surface roughness (n), maximum draining capacity in the middle layer (T_d), lateral transmissivity (T_i), interflow recession coefficient (m_i), base-flow recession coefficient (K_b), groundwater recharge or percolation (P_r) and bypass flow rate (Q_{by}). For the root zone storage, there are two ways to reduce the storage. One way is the evapotranspiration, which is turned off as well. The other way is the quick bypass flow (Q_{by}) from the root zone to the bottom layer when the saturation exceeds 0.6. When the storage is filled by precipitation, the surplus rainfall infiltrates into the middle layer. However, the infiltrating water depends

HESSD
10, 855–893, 2013

on the remaining space in the middle layer or on the maximum draining capacity T_d. Therefore, the saturation excess runoff can be described as follows:

$$\delta_i = \begin{cases} P_i - D_i & \text{if } D_i < T_d \\ P_i - T_d & \text{if } T_d > D_i \end{cases} \quad (4)$$

where P_i and D_i are the rainfall on that cell [L] and the local soil moisture deficit [L], respectively. δ_i is the surplus rainfall [L], which transforms to the surface runoff. As mentioned earlier, we also used the diffusive transport approach in TOPMODEL.

For the middle layer, the local soil moisture deficit D_i can be estimated by

$$D_i = \overline{D} + m_i \left(\gamma - \ln \left(\frac{\alpha_i}{T_i \cdot \tan \beta_i} \right) \right) \quad (5)$$

where γ is the mean value of the topographic index $\ln(a/T_i \tan\beta)$ over the catchment area. Parameter T_i in the topographic index is the lateral transmissivity as the soil is saturated [$L^2 T^{-1}$]. a is the specific contributing area defined as the drainage area per unit contour length [L], and tan β is the local gradient [–]. This equation uses the difference between the local topographic index and the average topographic indexes to estimate the possible local soil moisture deficit everywhere when the recession coefficient is given. Therefore, the subsurface runoff for each time step can be estimated by the following recession curve function:

$$Q_i = Q_0 \cdot \exp \left(-\frac{\overline{D}}{m_i} \right) \quad (6)$$

where Q_i is the interflow [$L^3 T^{-1}$] and $Q_0 = A \cdot \exp(-\gamma)$ is the discharge when the average soil moisture deficit is zero.

For the base flow, the same linear reservoir concept is applied to simulate the base flow as follows:

$$Q_b = S_b K_b \quad (7)$$

HESSD
10, 855–893, 2013

where Q_b and K_b are the base flows [L^3T^{-1}]. S_b [L] and K_b [L^2T^{-1}] are the states of the storage and the recession, respectively. The initial S_b can be derived from the initial observed discharge at time $t = 0$. The above three flows compose the stream discharge at the catchment outlet.

The two models show different model structures, particularly in the surface flow generation. The TOPMODEL generates the surface flow followed by the saturation excess runoff. The saturation in the middle layer is the key factor that controls the generation of the surface runoff. However, the HBV model separates the rainfall into root zone and inter-flow storage through the effective precipitation calculation, which is proportional to the soil moisture content and shape factor. In other words, the effective precipitation is the valve that controls and allows the recharge into interflow storage before the fully saturation of root zone. In addition, the surface flow occurs only when the water level in the interflow storage is higher than the threshold L, which means that the surface flow in HBV is controlled by threshold L, and the maximum interflow is somewhat limited. Meanwhile, we introduced the same base-flow governing equation to the two models to investigate the model behavior in the two different structures. The experiment design can aid us in understanding more about the model behaviors. Further, the sensitivities of the parameters were also evaluated to clarify the role of the allocation of the three flows. Hydrograph shapes, runoff volumes, and correlation coefficient were the performance measured used to discuss. Finally, the two rainstorms, supplemented by the intensive geochemical dataset for the stream flow compositions, were used to validate the simulated compositions.

2.3 Calibration and performance evaluation

In hydrological modeling, calibration is intensively used to determine the unknown and/or non-measurable parameters by ranking the performance measure between simulations and observations. However, many previous studies showed that no unique performance measure is better suited than another for the calibration of a model (Gupta

HESSD
10, 855–893, 2013

et al., 1998; Yapo et al., 1998; Madsen, 2000; Vrugt et al., 2003a,b); therefore, the multi-objective calibration has been proposed and applied widely. For the multi-objective calibration, the simulations laid on the Pareto front can be regarded as the best simulations, and the corresponding parameters are good candidates for further applications (e.g. parameter uncertainty estimation). Here, we use two efficiency coefficients as performance measure for the calibration. One efficiency coefficient is Nash_EC (proposed by Nash and Sutcliffe, 1970). This widely used coefficient (Eq. 8) varies from negative infinity to unity, where unity represents a perfect match and zero indicates that the simulation performance is identical to the expected value (mean) of the observations. However, this coefficient uses the squared difference between simulation and observation, which lead to high sensitivity in the high flow. To consider the low-flow properly, a variant Nash_EC$_{log}$, which transfers the simulated and observed discharges into a logarithmic scale, is applied as the other performance measure. In the present study, over 80 000 parameter sets were generated by the uniform or log-uniform distribution for the parameters required by the two models. The best simulations and the corresponding parameter sets, defined as the highest values of the Nash_EC and Nash_EC$_{log}$, are selectedfor further discussion.

$$\text{Nash\_EC} = 1 - \frac{\sum_{i=1}^{T}(Q_{\text{sim,i}} - Q_{\text{obs,i}})^2}{\sum_{i=1}^{T}(Q_{\text{sim,i}} - \overline{Q_{\text{obs,i}}})^2} \quad (8)$$

where Q_{sim} and Q_{obs} are the simulated and observed discharges, respectively, and T is the total time step during the evaluation period.

In addition to the two performance measures for calibration, we also used the following three indexes, namely, Nash_EC, EQV, and CC, to show the extent of the agreement between simulations and observations. EQV refers to the ratio of the simulated total volume over the observed total discharge volume. This index is useful in investigating the volume bias between observations and simulations, which is important for irrigation, reservoir operation, and flood control. CC is the correlation coefficient that represents the correlation between simulations and observations. Notably, a high CC

HESSD
10, 855–893, 2013

with poor EQV indicates that the simulation has a highly similar shape with the observations but with biases in the runoff volume simulation. Based on the three indexes, the model-derived simulations in terms of hydrograph shape, volume, and correlation can be assessed comprehensively.

3 Results

HBV- and TOPMODEL-derived simulations

After the intensive simulations and calibration, the performances of Nash_EC and Nash_EC$_{log}$ for the HBV- and TOP-derived simulations are shown in Fig. 3. In general, the overall Nash_EC and Nash_EC$_{log}$ values were scattered in an awl shape, and the maximum values met at approximately 0.65 in both axes for the two models. Two issues were addressed. One is that the Pareto front may not exist if the two performance measures are intrinsically similar. Therefore, we selected the best 15 simulations (the highest values of the sum of the two measures) as the representative simulations, and their corresponding parameter sets were regarded as the well-performed sets for each model (discussed later). The other is that both models could simulate the rainstorm fairly well; the overall Nash_EC and Nash_EC$_{log}$ values were higher than 0.6, showing a good agreement with the two model-derived simulations and observations. The detailed simulation results are tabulated in Table 2. In the HBV-derived simulations, the Nash_EC values varied from 0.16 to 0.91 with a mean of 0.70. For the TOPMODEL, the Nash_EC values ranged from 0.10 to 0.89 with a mean of 0.64. In general, the HBV-derived simulations were slightly better than the TOP-derived simulations. The standard deviations for the HBV- and TOP-derived models were 0.22 and 0.19, respectively, showing a similar level of variations among events.

For EQV, the average performance of the two models was similar (0.92 and 0.93 for HBV and TOP, respectively). However, the range varied from 0.56 to 1.52 for HBV and from 0.68 to 1.20 for TOP, respectively, showing that TOPMODEL could make the

HESSD
10, 855–893, 2013

simulated volume more consistent (less variation) with observations. For the correlation coefficient, the maximum CC for HBV and TOP was as high as 0.97. However, the average CC for HBV and TOP was 0.94 and 0.88, respectively, which indicated that the HBV simulations might give a higher correlation than the TOP simulations. The standard deviation of the TOP-derived CC was larger than that of the HBV-derived CC. Obviously, the TOP-derived simulations were inconsistent with the observations compared with the HBV-derived simulations in terms of the correlation (e.g. hydrograph shape).

In summary, HBV could provide a slightly better simulation in terms of the hydrograph shape; however, it was more scattered in discharge volume than the TOP-derived simulations. In addition, comparison among events showed that the specific parameter set that performed some events well does not guarantee applicability for the all other events (Huang et al., 2009). Although the pursuit of higher performance measures (e.g. average Nash_EC and Nash_EC$_{log}$ in this study) is the main consideration of the calibration, pursuing the smaller variation that ensures that the parameter set can perform in all events (e.g. different hydrological conditions) in a broad perspective should also be emphasized. In this regard, we may increase the difficulty in choosing a model that only depends on a single criterion and limited events.

4 Discussions

4.1 Well-performed simulation and corresponding parameter sets

The well-performed simulations and the performance in terms of Nash_EC, EQV, and CC are illustrated to reveal the variation in the simulations among the rainstorms (Fig. 4). In Fig. 4a.1 and b.1, we could find that the Nash_EC values of the 15 well-performed simulations for each event were quite different. The HBV-derived simulation outperformed in the small to middle rainstorms, although it failed to simulate the two events (event nos. 4 and 5; the observed runoff volumes were 237.6 and 245.5,

HESSD
10, 855–893, 2013

respectively). Similarly, the TOP-derived simulations also outperformed in the small and middle rainstorm. However, TOPMODEL provided more scattered simulations for small events. For the correlation coefficient, the HBV model presented good and consistent simulations for all events (Fig. 4a.2). The higher correlation coefficient values indicated that the simulations and observations all agreed well in terms of hydrograph shape. By contrast, the TOP-derived simulations only showed fair values. The simulations for small events were highly divergent (Fig. 4b.2). Meanwhile, the differences among the selected simulations were inconsistent and fluctuating. For the runoff volume estimations, the HBV-derived simulations for small events were distinctly overestimated but were underestimated for large events (Fig. 4a.3). By contrast, the TOP-derived simulations held the runoff volume estimation well and remained consistent (Fig. 4a.3).

This comparison indicated that the TOP-derived simulations with regard to the hydrograph shape were not well performed (e.g. Nash_EC and CC). One possible interpretation is that TOPMODEL applied the variable source-area concept in the surface runoff generation. Once the biased precipitation pattern fell on saturated or unsaturated area, over- and underestimation of the surface runoffs occurred (Huang et al., 2011). In addition, our previous study showed that small rainstorm spatial patterns are more heterogeneous (Huang et al., 2012). We could expect that the hydrological models cannot simulate well such events. As for runoff volume estimation, the TOP-derived simulations can maintain the water balance better than that derived by HBV. Taking a closer look at the model structures would reveal that the runoff estimation by HBV strongly depends on the storage status and the yield parameters (e.g. K_s, K_i, and K_b); therefore, the runoff may not follow the concept of mass balance. In other words, HBV is more flexible in adjusting the simulated stream discharges. We cannot determine if the real watershed responses follow the mass balance or not. Therefore, the essentiality of mass balance assumption in the model structure can be discussed further in designing the next generation of hydrological models.

For the corresponding parameter sets, the retrieved parameter values were normalized to the upper and lower limits and linked to one another for showing the connectivity

HESSD
10, 855–893, 2013

(Fig. 5). This figure shows different parameter sets covering a considerable range of parameter values that could produce virtually equally good model simulations based on Nash_EC and Nash_EC$_{log}$. The parameters that are constrained within a limited range indicated that they are more sensitive and dominant (Madsen, 2000; Madsen et al., 2003). Meanwhile, the pattern of parameter connectivity represents the model behavior. In this figure, the ranges of parameters S_{rmax}, K_s, L, and K_b are limited in revealing the importance and sensitivity of these parameters in the HBV model. Meanwhile, all the parameter connectivities with similar tendency show the same model behavior in these simulations. For TOPMODEL, only parameters DE_i and K_{per} are sensitive. In addition, more than one kind of parameter connectivities could achieve similar performance. Such result raised an interesting issue. A model which can provide several interpretations (e.g. parameter connectivities) for a events is better? Or we need a model which only hives a fixed interpretation (maybe wrong)? Here, we want to highlight that the parameter sensitivity correlating to model flexibility in hydrological modeling also should be considered.

4.2 Comparison of HBV- and TOP-derived stream composition

The simulated three flows for all rainstorms are listed in Table 3. Overall, the proportions of the three HBV-derived flows among all events occupy 0.22, 0.29, and 0.49 for the surface flow, interflow, and base flow, respectively. By contrast, the TOP-derived flows for the surface flow, interflow, and base flow are 0.27, 0.50, and 0.23, respectively. In comparison, the base flow played a dominant role in simulating the stream discharge in the HBV model; however, TOPMODEL treated interflow as the major component for stream discharge.

To reveal the relationship between the flow proportions and rainstorm characteristics, the flow proportion and average rainfall intensity and the storm duration are shown in Figs. 6–8 for the surface flow, interflow, and base flow, respectively. Figure 6 shows that both simulated surface flow proportions increased from 0.1 to 0.5 with the increase in the average rainfall intensity from 2.0 to 11.0 mm h^{-1}. Meanwhile, both simulated

HESSD
10, 855–893, 2013

surface flow proportions decreased from 0.5 to 0.1 with the increase in the storm duration from 40 to 160 h. However, the variations among the well-performed simulations were different. The HBV-derived surface flows among events showed larger variation than those derived from TOPMODEL. Nevertheless, the consistent results in surface flow derived from the two model structures, even for extreme events, revealed that the surface flow proportions which increased and decreased with the average rainfall intensities and storm durations, were fairly reliable and even realistic.

For the interflow, the models showed discrepant relationships with the average rainfall intensity and storm duration (Fig. 7). The HBV model showed lesser interflow (~ 0.3) than TOPMODEL (~ 0.5). Meanwhile, the two model behaviors showed opposite responses to the storm duration. As the storm duration increased, the interflow of TOPMODEL increased from ~ 0.3 to 0.6. However, the interflow result of HBV showed a decreasing trend from ~ 0.4 to 0.15. Such contrasting behaviors were due to the model structures. Theoretically, TOPMODEL simulated the larger interflow as using the decrease in the average soil deficit decreases, which was also used to determine the variable source area. In our case, the maximum variable source area was approximately 30 to 65 %. Therefore, we can expect that TOPMODEL can give even larger interflow for more torrential rainstorms. By contrast, the HBV model simulates the interflow using the limited depth of L. When heavy rainfall exceeds L would surface runoff occurs and the inter-flow storage reduced rapidly. Therefore, the proportion of inter flow was relatively limited even when the rainstorm increases.

For the base flow, the responses of the two models showed patterns similar to the correlated simulated base flows with average rainfall intensity (Fig. 8). However, the HBV range was from 0.7 to 0.1, much wider than that derived from TOP (from 0.4 to 0.08). Meanwhile, the HBV-derived base flow increased with the increase in the storm duration; such relationship was not found in the TOPMODEL simulations. TOPMODEL showed consistent base flow (avg = 0.23; std. = 0.098) for all events. In the TOPMODEL structure, because the interflow responded to much water yield, the base flow did not have to change. By contrast, the HBV model matched the stream discharge

HESSD
10, 855–893, 2013

by enforcing more percolation. Therefore, the base flow was compelled to increase, particularly during extreme rainstorms, which indicates that HBV may be more suitable for watersheds with thin soil layer. By contrast, TOPMODEL is preferable for watersheds with thick soil layer. In this regard, we might speculate that the proper model choice should be based on the extensive spectrum of rainstorms and the extra environmental background, instead of intensive calibration. Meanwhile, such intercomparison between models also increased our understanding of the model structures and behaviors.

4.3 Comparison with chem-hydrograph

To determine the accuracy of the stream flow composition, the geochemical dataset was introduced independently. The stream flow composition derived from the end-member mixing analysis (EMMA) is shown in Fig. 9. This figure results from intensive sampling works. Lee et al. (2010, 2011, 2012) collected water samples in wells and soil columns for the end member of the base flow and interflow. Besides, they sampled the stream and rainwater at high frequency (~ 3 h interval) during rainstorms for the EMMA calculation. The chem-hydrographs of the three components after the EMMA are shown in Fig. 10a, b for event nos. 15 and 17, respectively, which show that the base flow was quite stable and only changed during the flood peak time. In general, the base flow occupied approximately 25 % of the total runoff. In contrast to the base flow, the interflow surged and diminished quickly. The values of the interflow were almost identical to the base flow. The remaining discharge was attributed to the surface flow. From the geochemical perspective, the surface flow was the most important component during the rainstorm period, which occupied approximately 40 to 50 % of the total runoff volume.

EMMA was recognized as a useful analysis tool for hydrograph separation, although the number and selection of geochemical tracers are sometimes questionable (Barthold et al., 2011; Carrera et al., 2004). Despite the uncertain proportion of discharge components and the objective identification of the end members, the result of

HESSD
10, 855–893, 2013

the stream composition, in terms of relative proportion, is roughly reliable. At least, such result provided another perspective for stream flow composition. More important, the time-series changes of the flows are relatively realistic. In this regard, the EMMA-derived stream composition could be a good reference for comparison with the model-derived ones.

The EMMA- and the model-derived results are listed in Table 4. The HBV model simulation shows that the interflow and base flow are dominant components for event nos. 15 and 17, respectively. By contrast, TOPMODEL always considers the interflow as the superior component; the surface flow was only secondary. No model yields the same EMMA-derived composition with regard to the proportion. From the quantity perspective, the TOP-derived surface flow shows a good agreement with that derived by EMMA. By contrast, the HBV-derived results in the interflow and base flow are closer to the EMMA-derived results than those derived by TOPMODEL, although the surface flow is underestimated.

Not only the quantity but also the response-time results are shown in Figs. 10 and 11 for event nos. 15 and 17, respectively. These two figures show that the HBV-simulated discharge is slightly underestimated, and TOPMODEL shows overestimation in the stream discharge. However, TOPMODEL exhibits a good agreement in the recession segment for the two events. For the interflow, the two models produce fair results, and HBV slightly outperforms. For the base flow, the HBV model simulates the base flow as a gentle dome. By contrast, the TOP-derived base flow shows a quick-response steep-bell shape. In the shape comparison, the TOPMODEL outperforms the HBV Model. However, a significant time lag of approximately 2 to 4 h is observed. In our case, the base flow responds with the stream discharge simultaneously. The base-flow could thus be considered a type of piston flow. In this regard, incorporating the piston flow theory into the hydrological models can improve the time lag, which aids in the interpretation of the base-flow.

HESSD
10, 855–893, 2013

5 Summary

Many hydrological models can simulate the stream flow satisfactory and plausibly. However, different runoff compositions can result in the similar discharges. Therefore, recent attention has shifted to model structures to ensure the accuracy of relevant inferences. In our study, the parameter connectivity representing the model interpretations is discussed. HBV presented consistent parameter connectivity; however, TOPMODEL achieved more than one kind of parameter connectivity, which implied that HBV preferred to give only one interpretation for the simulation, but TOPMODEL could yield more. Rethinking is thus necessary to identify which model structure is better.

In the comparison of the simulated components, both simulated surface flows which increased with the increase in the rainfall intensity and decreased with the increase in the storm duration should be realistic. Both base flows also showed the same patterns, although HBV always simulated a plentiful base flow. However, both models exhibited a contrasting relationship with the storm duration for the interflow. The HBV interflow decreased with the increase in duration. Because of the limited interflow storage, this model compelled to percolate much water to the base flow storage in order to match the stream discharge, which indicated that HBV could be more suitable for the environment of thin-soil or highly permeable soil mantle and TOP could be a better choice for catchments with thick soil. Compared with the EMMA-derived flows, there is a significant 2 to 4 h time lag was observed, which indicated that the real base-flow responses are faster than the models have presented. Possibly, an explicit consideration of the piston-flow characteristics in the base flow should be incorporated to improve the time lag and aid in the interpretation of the base flow.

Obviously, intercomparison between models under a wide spectrum of rainstorms is a good way to understand better the model behaviors. Meanwhile, the independent geochemical data (e.g. EMMA-derived components) provides another perspective in examining the model behaviors. Undoubtedly rejecting a model completely is difficult. By contrast, it is very likely that more than one model structure can capture the stream

HESSD
10, 855–893, 2013

flow and tracer dynamics simultaneously when the rainstorm cases and environment background are insufficient. In this regard, we must rethink the model structure and the watershed characteristics as using a hydrological model.

Acknowledgement. This study was supported by Taiwan National Science Council and National Taiwan University under grants NSC 101-2116-M-002-017, NSC 100-2621-M-002-027-MY3, NSC 101-2923-B-001-MY3, and NTU 10R70604-2. The authors also appreciated Taiwan Power Company and Shei-Pa National Park providing the hydrological data and well samples. Ms. Lee, Li-Chin's work in drawing figures was appreciated.

References

Aghakouchak, A. and Habib, E.: Application of a conceptual hydrologic model in teaching hydrologic processes, Int. J. Engin. Educ., 26, 963–973, 2010.

Barthold, F. K., Tyralla, C., Schneider, K., Vachè, K. B., Frede, H.-G., and Breuer, L.: How many tracers do we need for end member mixing analysis (EMMA)? A sensitivity analysis, Water Resour. Res., 47, W08519, doi:10.1029/2011WR010604, 2011.

Bergström, S.: The HBV Model – its Structure and Applications, SMHI RH no. 4, Norrköping, Sweden, 1992.

Bergström, S. and Forsman, A.: Development of a conceptual deterministic rainfall-runoff model, Nord. Hydrol., 4, 147–170, 1973.

Beven, K. J.: The limits of splitting: hydrology, Sci. Total Environ., 183, 89–97, 1996.

Beven, K. J. (Ed.): Revisiting the problem of model choice, in: Rainfall-Runoff Mofelling The Primer, John Wiley and Sons, New York, 297–304, 2001.

Beven, K. J. and Freer, J.: Equifinality, data assimilation, and uncertainty estimation in mechanistic modeling of complex environmental systems using the GLUE methodology, J. Hydrol., 249, 11–29, 2001.

Beven, K. J. and Kirkby, M. J.: A physically based variable contributing area model of basin hydrology, Hydrol. Sci. Bull., 24, 43–69, 1979.

Blöschl, G., Reszler, C., and Komma, J.: A spatially distributed flash flood forecasting model, Environ. Model. Softw., 23, 464–478, 2008.

HESSD

10, 855–893, 2013

Burns, D. A., McDonnell, J. J., Hooper, R. P., Peters, N. E., Freer, J. E., Kendall, C., and Beven, K.: Quantifying contributions to storm runoff through end-member mixing analysis and hydrologic measurements at the Panola Mountain Research watershed (Georgia, USA), Hydrol. Process., 15, 1903–1924, 2001.

Carrera, J., Vázquez-Suñé, E., Castillo, O., and Sánchez-Vila, X.: A methodology to compute mixing ratios with uncertain end-members, Water Resour. Res., 40, W12101, doi:10.1029/2003WR002263, 2004.

Clark, M. P., Slater, A. G., Rupp, D. E., Woods, R. A., Vrugt, J. A., Gupta, H. V., Wagener, T., and Hay, L. E.: Framework for understanding structural errors (FUSE): a modular framework to diagnose differences between hydrological models, Water Resour. Res., 44, W00B02, doi:10.1029/2007WR006735, 2008.

Fenicia, F., McDonnell, J. J., and Savenije, H. H. G.: Learning form model improvement: on the contribution of complementary data to process understanding, Water Resour. Res., 44, W0619, doi:10.1029/2007WR006386, 2008.

Gupta, H. V., Sorooshian, S., and Yapo, P. O.: Toward improved calibration of hydrologic models: multiple and non-commensurable measures of information, Water Resour. Res., 34, 751–763, 1998.

Gupta, H. V., Clark, M. P., Vrugt, J. A., Abramowita, G., and Ye, M.: Towards a comprehensive assessment of model structural adequacy, Water Resour. Res., 48, W08301, doi:10.1029/2011WR011044, 2012.

Haberlandt, U., Klocking, B., Krysanova, V., and Becker, A.: Regionalisation of the base flow index from dynamically simulated flow components – a case study in the Elbe River Basin, J. Hydrol., 248, 35–53, 2001.

Huang, J. C., Kao, S. J., Hsu, M. L., and Lin, J. C.: Stochastic procedure to extract and to integrate landslide susceptibility maps: an example of mountainous watershed in Taiwan, Nat. Hazards Earth Syst. Sci., 6, 803–815, doi:10.5194/nhess-6-803-2006, 2006.

Huang, J.-C., Lee, T.-Y., and Kao, S.-J.: Simulating typhoon-induced storm hydrographs in subtropical mountainous watershed: an integrated 3-layer TOPMODEL, Hydrol. Earth Syst. Sci., 13, 27–40, 1doi:0.5194/hess-13-27-2009, 2009.

Huang, J. C., Kao, S. J., Lin, C. Y., Chang, P. L., Lee, T. Y., and Li, M. H.: Effect of subsampling tropical cyclone rainfall on flood hydrograph response in a subtropical mountainous catchment, J. Hydrol., 409, 248–261, doi:10.1016/j.jhydrol.2011.08.037, 2011.

HESSD
10, 855–893, 2013

Huang, J. C., Yu, C. K., Lee, J. Y., Cheng, L. W., Lee, T. Y., and Kao, S. J.: Linking typhoon tracks and spatialrainfall patterns for improvi ng flood lead time predictions over a mesoscale mountainous watershed, Water Resour. Res., 48, W09540, doi:10.1029/2011WR011508, 2012.

Johnson, M. S., Coon, W. F., Mehta, V. K., Steenhuis, T. S., Brooks, E. S., and Boll, J.: Application of two hydrologic models with different runoff mechanisms to a hillslope dominated watershed in the northeastern US: a comparison of HSPF and SMR, J. Hydrol., 284, 57–76, 2003.

Katsuyama, M., Ohte, N., and Kobashi, S.: A three-component end-member analysis of streamwater hydrochemistry in a small Japan forested headwater catchment, Hydrol. Process., 15, 249–260, 2001.

Krysanova, V., Bronstert, A., and Müller-Wohlfeil, D.-I.: Modelling river discharge for large drainage basins: from lumped to distributed approach, Hydrolog. Sci. J., 44, 313–33, 1999.

Lin, Y.-F., Lin, C.-Y., Chou, W.-C., Lin, W.-T., Tsai, J.-S., and Wu, C.-F.: Modeling of riparian vegetated buffer strip width and placement: a case study in Shei Pa National Park, Taiwan, Ecol. Eng., 23, 327–339, 2004.

Lindström, G., Johansson, B., Persson, M., Gardelin, M., and Bergström, S.: Development and test of the distributed HBV-96 hydrological model, J. Hydrol., 201, 272–288, 1997.

Lee, T. Y.: Study on Integration of Monitoring and Modeling for Analyzing the Effects of Land Use Changes on Water Quality and Stream Temperature in Chichiwan Creek, Doctoral Dissertation, Graduate Institute of Bioenvironmental Systems Engineering, National Taiwan University, Taipei, Taiwan, 2010.

Lee, T. Y., Huang, J. C., and Kao, S. J.: Typhoon hydrograph separation in the mountainous watershed of Taiwan, Asia Oceania Geosciences Society 2011, 8th Annual Meeting, August, Taipei, Taiwan, 2011.

Lee, T.-Y., Huang, J.-C., Kao, S.-J., and Tung, C.-P.: Temporal variation of nitrate and phosphate transport in headwater catchments: the hydrological controls and landuse alteration, Biogeosciences Discuss., 9, 13211–13241, doi:10.5194/bgd-9-13211-2012, 2012.

Liu, Y. B., Gebremeskel, S., De Smedt, F., Hoffman, L., and Pfister, L.: A diffusive approach for flow routing in GIS based flood modeling, J. Hydrol., 283, 91–106, 2003.

Madsen, H.: Automatic calibration of a conceptual rainfall-runoff model using multiple objectives, J. Hydrol., 235, 276–288, 2000.

HESSD
10, 855–893, 2013

Madsen, H.: Parameter estimation in distributed hydrological catchment modelling using automatic calibration with multiple objectives, Adv. Water Resour., 26, 205–216, 2003.
McMillan, H., Tetzlaff, D., Clark, M., and Soulsby, C.: Do time-variable tracers aid the evaluation of hydrological model structure? A multimodel approach, Water Resour. Res., 48, W05501, doi:10.1029/2011WR011688, 2012.
Michaud, J. and Sorooshian, S.: Comparison of simple versus complex distributed runoff models on a midsized semiarid watershed, Water Resour. Res., 30, 593–605, 1994.
Nash, J. E. and Sutcliffe, J. V.: River flow forecasting through conceptual models, 1. A discussion of principles, J. Hydrol., 10, 282–290, 1970.
Perrin, C., Michel, C., and Andreassian, V.: Does a large number of parameters enhance model performance? Comparative assessment of common catchment model structures on 429 catchments, J. Hydrol., 242, 275–301, 2001.
Pokhrel, P. and Gupta, H. V.: On the ability to infer spatial catchment variability using streamflow hydrographs, Water Resour. Res., 47, W08534, doi:10.1029/2010WR009873, 2011.
Reed, S., Koren, V., Smith, M., Zhang, Z., Moreda, F., Seo, D.-J., and DMIP participants: Overall distributed model intercomparison project results, J. Hydrol., 29, 27–60, 2004.
Refsgaard, J. C. and Henriksen, H. J.: Modelling guidelines – terminology and guiding principles, Adv. Water Resour., 27, 71–82, 2004.
Sayama, T. and McDonnell, J. J.: A new time-space accounting scheme to predict stream water residence time and hydrograph source components at the watershed scale, Water Resour. Res., 45, W07401, doi:10.1029/2008WR007549, 2009.
Sorooshian, S. and Dracup, J. A.: Stochastic parameter estimation procedures for hydrologic rainfall-runoff models: correlated and heteroscedastic error cases, Water Resour. Res., 16, 430–442, 1980.
Valeo, C. and Moin, S. M. A.: Hortaonian and variable source area modeling in urbanizing basins, J. Hydrol. Eng., 6, 328–335, 2001.
Vrugt, J. A., Gupta, H. V., Bastidas, L. A., Bouten, W., and Sorooshian, S.: Effective and efficient algorithm for multiobjective optimization of hydrologic models, Water Resour. Res., 39, 1214, 2003a.
Vrugt, J. A., Gupta, H. V., Bastidas, L. A., Bouten, W., and Sorooshian, S.: A shuffled complex evolution metropolis algorithm for optimization and uncertainty assessment of hydrologic model parameters, Water Resour. Res., 39, 1201, 2003b.

HESSD
10, 855–893, 2013

Wagener, T., Sivapalan, M., Troch, P. A., McGlynn, B. L., Harman, C. J., Gupta, H. V., Kumar, P., Rao, P. S. C., Basu, N. B., and Wilson, J. S.: The future of hydrology: an evolving science for a changing world, Water Resour. Res., 46, W05301, doi:10.1029/2009WR008906, 2010.

Weiler, M., McGlynn, B. L., McGuire, K. J., and McDonnell, J. J.: How does rainfall become runoff? A combined tracer and runoff transfer function approach, Water Resour. Res., 39, 1315, doi:10.1029/2003WR002331, 2003.

Winchell, M., Gupta, H. V., and Sorooshian, S.: On the simulation of infiltration- and saturation-excess runoff using radar-based rainfall estimates: effects of algorithm uncertainty and pixel aggregation, Water Resour. Res., 34, 2655–2670, 1998.

Yapo, P. O., Gupta, H. V., and Sorooshian, S.: Multi-objective global optimization for hydrologic models, J. Hydrol., 204, 83–97, 1998.

HESSD
10, 855–893, 2013

Table 1. The rainstorm characteristics in Chi-Chia-Wen catchment since 1986.

Event no.	Date	Duration (h)	Rainfall (mm)	Max. RI** ($mm\,h^{-1}$)	Runoff volume (mm)	Peak flow ($mm\,h^{-1}$)	RC***
1	1986/09/18	108	316.0	26.5	140.3	5.4	0.44
2	1986/08/22	95	247.2	15.6	69.9	2.9	0.28
3	1989/09/10	120	595.3	38.4	330.7	13.4	0.56
4	1990/09/07	96	454.9	28.6	237.6	7.9	0.52
5	1990/08/18	121	425.6	24.9	245.5	6.9	0.58
6	1990/06/22	105	359.7	28.8	132.2	3.7	0.37
7	1996/07/30	110	451.1	27.3	363.8	13.5	0.81
8	1997/08/28	90	228.5	17.5	120.8	5.2	0.53
9	1998/10/15	120	273.6	23.3	128.6	2.8	0.47
10	2000/08/22	94	398.8	25.7	107.3	3.5	0.27
11	2004/08/23	80	452.9	25.9	351.1	17.5	0.78
12	2004/07/02	96	431.3	35.3	112.3	4.5	0.26
13	2005/08/31	40	426.9	39.5	198.3	17.4	0.46
14	2006/06/08	144	409.4	20.3	247.9	5.5	0.61
15*	2007/08/17	87	490.2	38.5	334.3	13.9	0.68
16	2007/09/17	97	184.5	15.0	75.8	2.3	0.41
17*	2007/10/05	120	629.7	35.4	403.2	15.4	0.64
18	2008/07/17	90	200.0	21.7	93.0	2.6	0.47
19	2008/09/12	144	836.4	10.7	672.6	11.6	0.80
20	2008/09/27	91	672.9	33.3	483.4	16.5	0.72
21	2009/08/06	154	829.4	22.0	622.6	11.6	0.75
22	2009/10/05	72	220.5	14.9	37.8	2.0	0.17
23	2010/09/19	72	253.1	28.9	103.7	4.9	0.41
	Average	102	430.0	26.1	245.1	8.4	0.52

* meant the events had the chem-hydrographs for validation,
** Max RI was the maximum rainfall intensity during the event,
*** RC, runoff coefficient indicated the total runoff over the total rainfall.

HESSD
10, 855–893, 2013

Table 2. The HBV- and TOP-derived simulations evaluated by EC, EQV, and CC.

Event no.	HBV Model			TOP Model		
	Nash EC	EQV	CC	Nash EC	EQV	CC
1	0.87	0.91	0.96	0.86	0.91	0.94
2	0.72	1.37	0.97	0.68	0.81	0.86
3	0.80	0.72	0.97	0.89	0.84	0.95
4	0.16	0.56	0.96	0.79	0.85	0.93
5	0.25	0.56	0.97	0.78	0.76	0.97
6	0.84	1.07	0.97	0.67	1.11	0.93
7	0.81	0.73	0.95	0.75	0.78	0.92
8	0.77	0.86	0.92	0.47	0.87	0.74
9	0.86	0.92	0.96	0.43	0.83	0.73
10	0.91	0.97	0.97	0.61	0.84	0.82
11	0.84	0.89	0.95	0.88	1.05	0.97
12	0.66	1.11	0.87	0.54	1.06	0.89
13	0.69	0.98	0.84	0.70	1.17	0.89
14	0.56	0.79	0.92	0.78	1.00	0.92
15*	0.82	0.78	0.96	0.61	1.00	0.94
16	0.75	1.14	0.93	0.60	0.94	0.83
17*	0.83	0.82	0.97	0.81	1.15	0.98
18	0.85	1.06	0.95	0.10	0.68	0.63
19	0.43	0.64	0.92	0.59	0.95	0.90
20	0.89	0.86	0.96	0.40	1.20	0.94
21	0.60	0.70	0.92	0.69	0.88	0.86
22	0.30	1.52	0.95	0.62	0.82	0.85
23	0.78	1.14	0.97	0.38	0.80	0.75
Average	0.70	0.92	0.94	0.64	0.93	0.88
Std.	0.22	0.24	0.03	0.19	0.14	0.09

* Note that the value for each event is the average of the representative simulations.

HESSD
10, 855–893, 2013

Table 3. The proportion of the simulated surface-, inter-, and base-flows derived from the two models.

Event	HBV Model derived			TOP Model derived		
no.	Surface flow	Inter flow	Base flow	Surface flow	Inter flow	Base flow
1	0.26	0.31	0.43	0.30	0.51	0.19
2	0.17	0.32	0.51	0.26	0.46	0.28
3	0.27	0.31	0.41	0.33	0.50	0.16
4	0.17	0.23	0.60	0.21	0.56	0.23
5	0.15	0.22	0.63	0.16	0.57	0.27
6	0.18	0.27	0.55	0.18	0.56	0.26
7	0.34	0.35	0.31	0.44	0.44	0.13
8	0.14	0.26	0.60	0.10	0.58	0.32
9	0.11	0.23	0.66	0.10	0.55	0.35
10	0.26	0.32	0.42	0.32	0.49	0.18
11	0.41	0.39	0.20	0.51	0.41	0.07
12	0.18	0.30	0.52	0.24	0.56	0.20
13	0.43	0.40	0.17	0.53	0.39	0.08
14	0.07	0.16	0.77	0.09	0.54	0.37
15*	0.31	0.42	0.27	0.39	0.46	0.16
16	0.09	0.24	0.67	0.09	0.52	0.40
17*	0.29	0.31	0.40	0.30	0.55	0.15
18	0.11	0.25	0.64	0.16	0.46	0.38
19	0.25	0.27	0.48	0.27	0.58	0.15
20	0.36	0.34	0.31	0.40	0.44	0.16
21	0.20	0.25	0.55	0.22	0.61	0.17
22	0.13	0.29	0.58	0.27	0.38	0.36
23	0.26	0.35	0.39	0.45	0.30	0.24
Average	0.22	0.29	0.49	0.27	0.50	0.23
Std.	0.10	0.06	0.16	0.13	0.08	0.10

HESSD
10, 855–893, 2013

Table 4. Stream discharge composition derived from two models and EMMA.

Event	Flow type	Chem-hydrograph		HBV Model		TOP Model	
		Amount ($m^3 s^{-1}$)	Proportion (%)	Amount ($m^3 s^{-1}$)	Proportion (%)	Amount ($m^3 s^{-1}$)	Proportion (%)
No. 15	Surface-flow	3949	40.5	2428	31.1	3711	38.5
	Inter-flow	2905	29.8	3305	42.3	1689	45.5
	Base-flow	2896	29.7	2076	26.6	1537	16.0
No. 17	Surface-flow	5562	47.3	2690	29.2	4116	30.4
	Inter-flow	2928	24.9	2837	30.8	7460	55.1
	Base-flow	3269	27.8	3685	40.0	1963	14.5

HESSD
10, 855–893, 2013

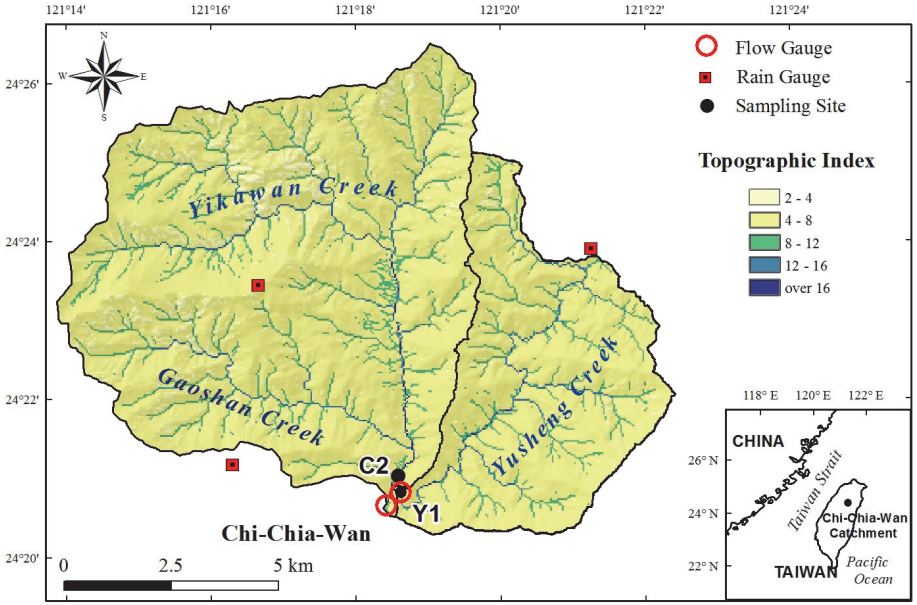

Fig. 1. The landscape, stream network and topographic index pattern within the Chi-Chia-Wen catchment. The raingages, flow stations are labeled by red square and black dot.

HESSD
10, 855–893, 2013

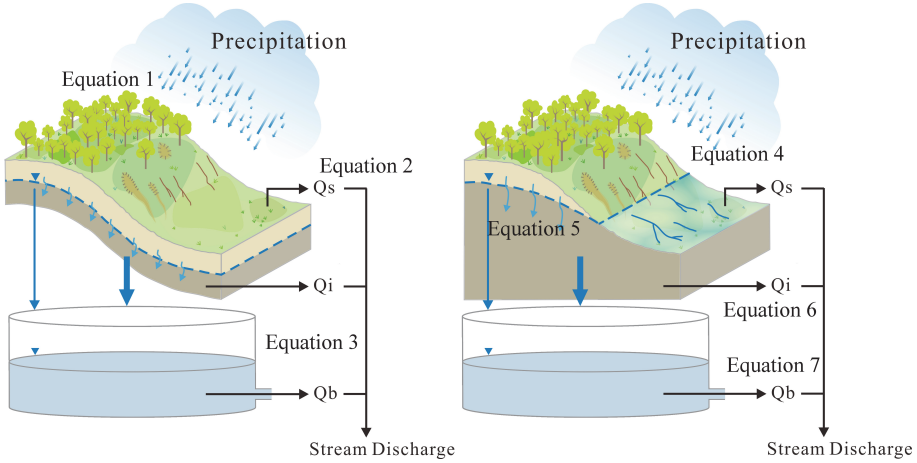

Fig. 2. The conceptual diagrams of HBV-Model (left panel) and TOP-Model (right panel).

HESSD
10, 855–893, 2013

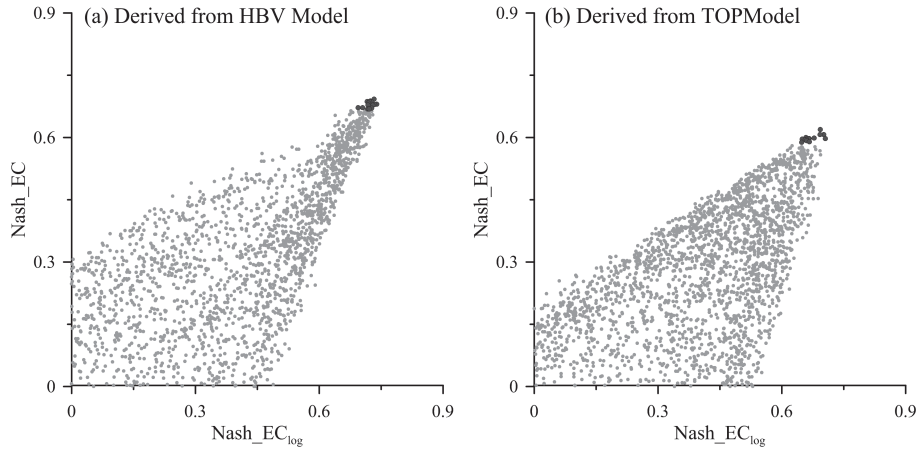

Fig. 3. The Nash EC and Nash_EC$_{log}$ values corresponding to the generated parameter sets in calibration process. The HBV-derived and TOP-derived results are shown in left and right panel, respectively. The x-axis and y-axis represent the Nash EC$_{log}$, and Nash EC, respectively. The gray circles represent the simulations partly and the black ones are the best 15 simulations sorted out by the equally weighted ranking.

HESSD
10, 855–893, 2013

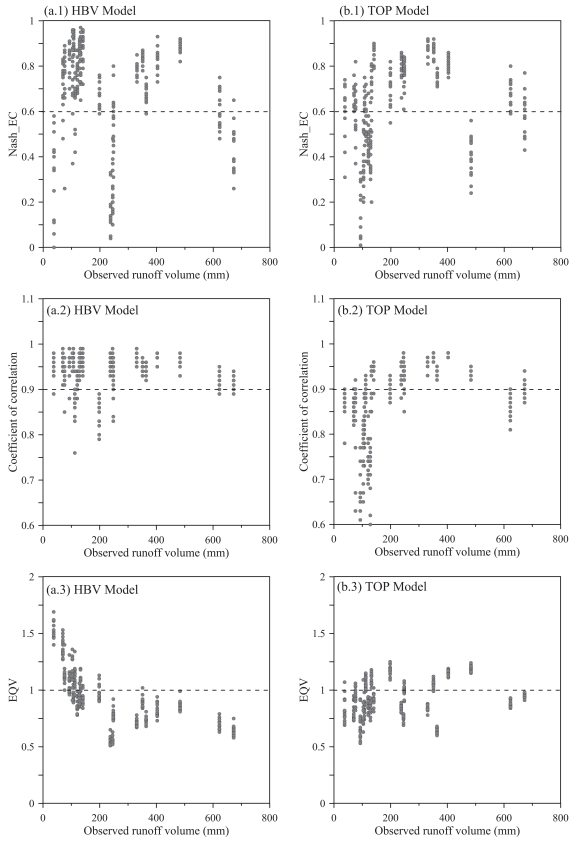

Fig. 4. The performances of the best HBV- **(a)** and TOP-derived simulations **(b)**, respectively, against the rainstorm magnitude in terms of observed runoff volume. The performance measure of Nash EC, coefficient of correlation, and volume bias are shown in the upper, middle, and bottom panels, respectively. The dash lines are shown for reference.

HESSD
10, 855–893, 2013

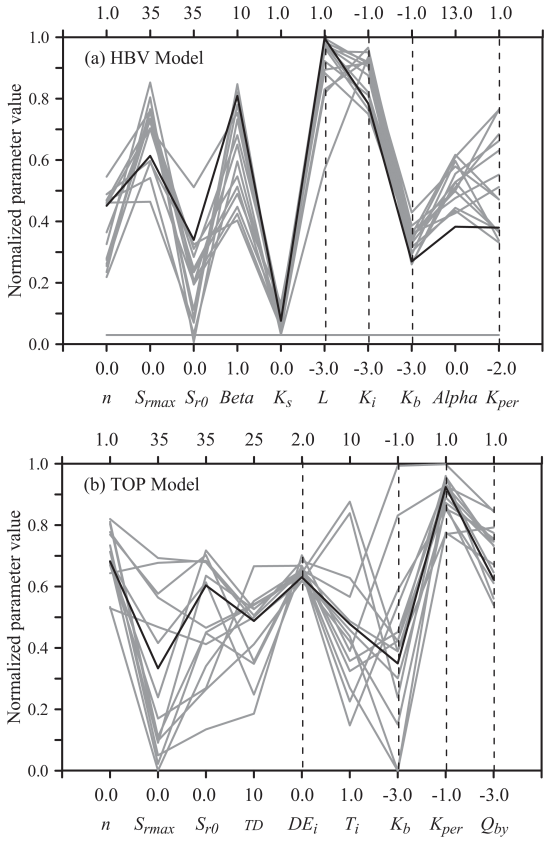

Fig. 5. Normalized range of parameter values of the 15 best simulations (gray lines) for HBV Model **(a)** and TOP Model **(b)**. The vertical dashed lines represent the parameter in logarithmic scale. The black lines indicate the best one for the two models.

HESSD
10, 855–893, 2013

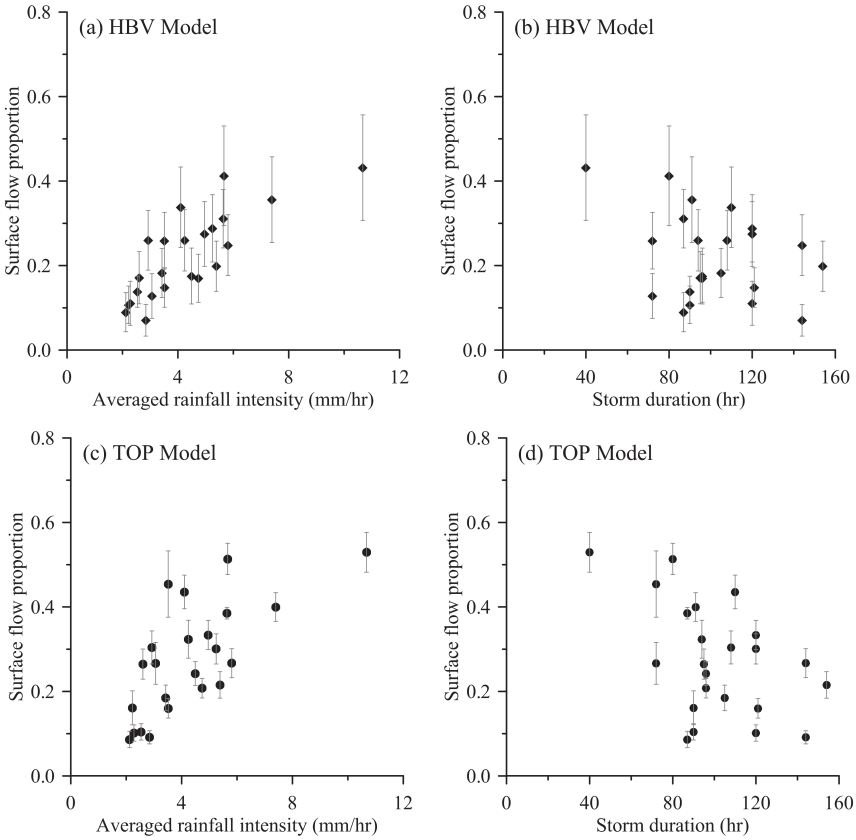

Fig. 6. The variation of HBV-derived surface flow against averaged rainfall intensity **(a)** and storm duration **(b)**. The variation of TOP-derived surface flow against averaged rainfall intensity **(c)** and storm duration **(d)**. The black dot and gray line represent the mean and the standard deviation among the best simulations.

HESSD
10, 855–893, 2013

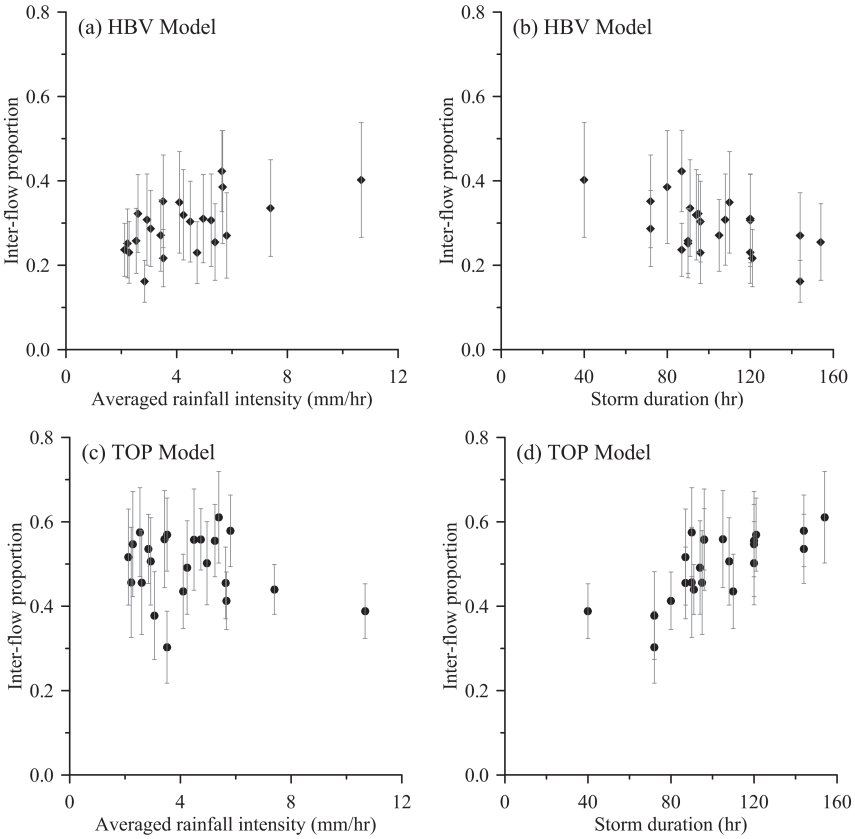

Fig. 7. The variation of HBV-derived inter-flow against averaged rainfall intensity **(a)** and storm duration **(b)**. The variation of TOP-derived inter-flow against averaged rainfall intensity **(c)** and storm duration **(d)**. The black dot and gray line represent the mean and the standard deviation among the best simulations.

HESSD
10, 855–893, 2013

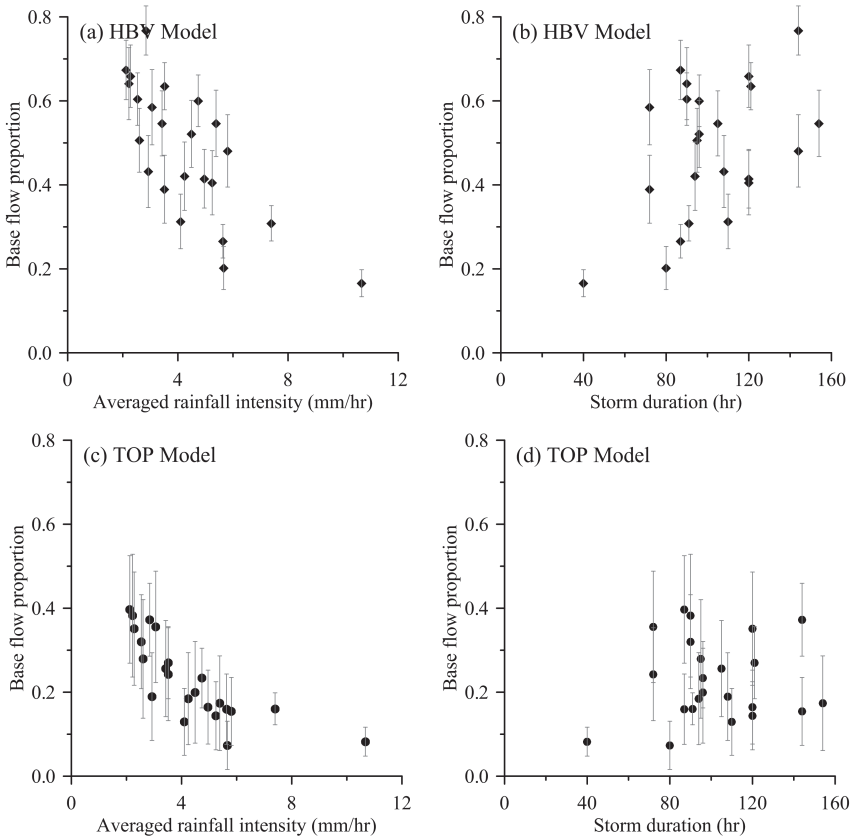

Fig. 8. The variation of HBV-derived base-flow against averaged rainfall intensity **(a)** and storm duration **(b)**. The variation of TOP-derived base-flow against averaged rainfall intensity **(c)** and storm duration **(d)**. The black dot and gray line represent the mean and the standard deviation among the best simulations.

HESSD
10, 855–893, 2013

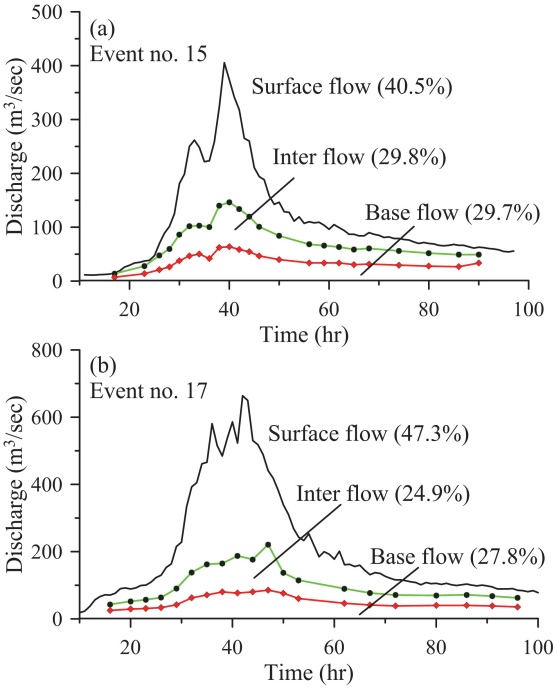

Fig. 9. The EMMA-estimated three discharge components of event no. 15 and no. 17 are shown in **(a)** and **(b)** for event no. 15 and 17, respectively. The black lines represented the observed stream discharge. The green and red lines indicate the estimated inter- and base-flow derived from EMMA (seeing text in Sect. 4.3 for details).

HESSD
10, 855–893, 2013

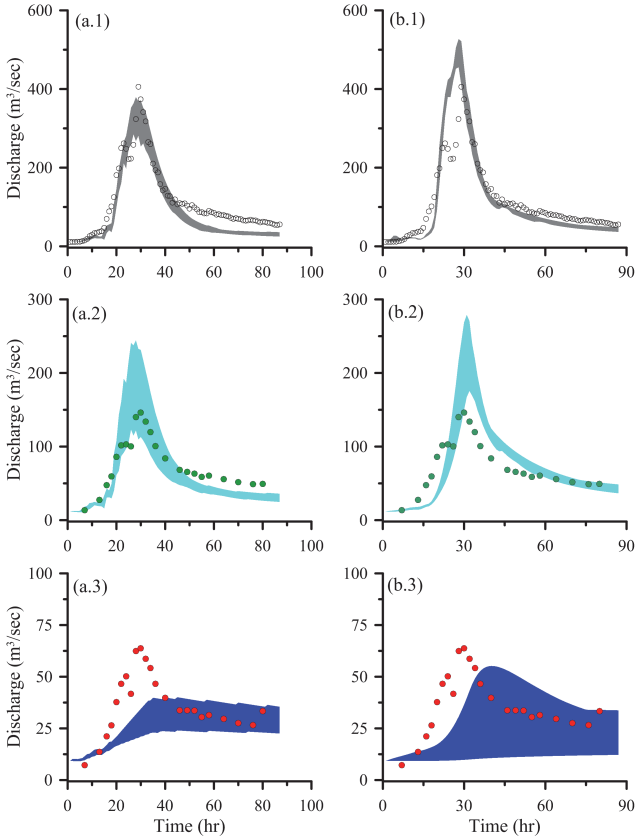

Fig. 10. Comparison between the measured stream discharges (event no. 21) and the best 15 simulations derived from HBV model **(a.1)** and TOP model **(b.1)**. The comparison of interflow derived from mixing analysis (green dot) with the simulated inter-flows (sky blue zone) derived from HBV model **(a.2)** and TOP model **(b.2)**, respectively. The comparison of baseflow derived from mixing analysis (red dots) with the simulated inter-flows (blue zone) derived from HBV model **(a.3)** and TOP model **(b.3)**, respectively.

HESSD
10, 855–893, 2013

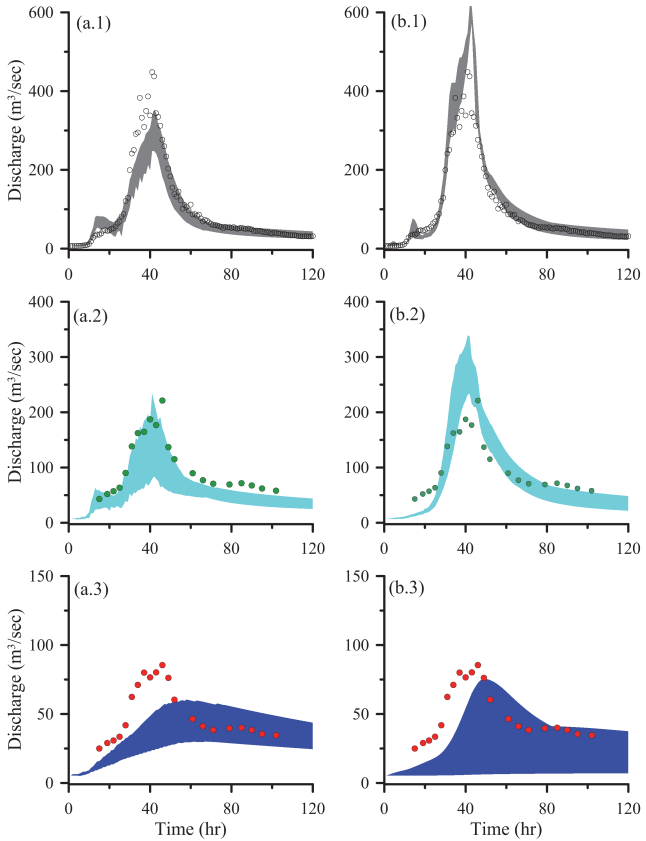

Fig. 11. Comparison between the measured stream discharges (event no. 23) and the best 15 simulations derived from HBV model **(a.1)** and TOP model **(b.1)**. The comparison of interflow derived from mixing analysis (green dotc) with the simulated inter-flows (sky blue zone) derived from HBV model **(a.2)** and TOP model **(b.2)**, respectively. The comparison of baseflow derived from mixing analysis (red dots) with the simulated inter-flows (blue zone) derived from HBV model **(a.3)** and TOP model **(b.3)**, respectively.

HESSD
10, 855–893, 2013